PEP-148

Large-Solid-Angle Detector for Charged and Neutral Particles

A. Barbaro-Galtieri, J. Kadyk, T. Mast, J. Nelson, A. Odian, D. Yount

ABSTRACT

The possibility of a PEP detector suitable for both charged and neutral particles is investigated. Such a detector would be well suited to studies of QED, hadronic final states and searches for new particles. The detector would consist of a central solenoidal magnet (conventional or superconducting) with drift chambers for charged particle momentum measurements and an outside system of shower detectors (Pb-glass or liquid argon) to measure both position and energy of the γ rays. High pressure Cerenkov counters can be introduced between the solenoid and the γ detectors in order to identify charged particles with a K-π separation up to 2 GeV/c and a p-π separation up to 4 GeV/c. In addition, at small angles a system of Cerenkov counters, toroidal magnets with internal drift chambers,and shower detectors can be added to measure the momenta and directions of charged and neutral particles.

Table of Contents

I. Introduction

The main purpose of the facility considered here is to detect both neutral and charged particles over as large a solid angle as possible. The following properties would be desirable in principle:

(a) large solid angle coverage for both particle measurements and triggering,

(b) good momentum and direction measurement of the charged particles, i.e., small $\frac{\Delta p}{p}$, over a large momentum range,

(c) good charged particle identification, i.e. π-K and π-p separation, over a wide momentum range,

(d) good efficiency for neutral particles detection: n, $\bar{n}$, γ,

(e) good energy and position measurements for neutral particles.

It is also desirable on the other hand to keep the size, cost and power consumption at a reasonable level; therefore compromises between the various possibilities must be made.

A brief discussion of the physics problems to be studied with such a detector is necessary at this point in order to decide quantitatively on the requirements (a) - (e).

II. Physics Motivation

A. $e^+e^- \to$ Hadrons

Many questions have been raised by recent CEA and SPEAR results on hadron production. At PEP we want to measure:

(i) total cross section,

(ii) partial cross sections for individual reactions ($e^+e^- \to c\pi^\pm$, $n\pi^\circ$, $e^+e^- \to c\pi^\pm + n\pi^\circ + aK + b\bar{K}$, $e^+e^- \to c\pi^\pm + n\pi^\circ + e\eta$, $e^+e^- \to N + \bar{N} + c\pi$ etc...),

(iii) inclusive π, K, N spectra for both charged and neutral particles,

(iv) exclusive reactions like $e^+e^- \to \rho^+\rho^-$, $\omega\pi^\circ$, $\rho^\pm A_2^\mp$, etc.,

(v) particle correlations (Is there any jet structure or are the hadrons produced isotropically?),

(vi) two γ processes, that is $e^+e^- \to e^+e^-$ + hadrons.

All of these types of measurements, except (vi), are directly relevant to the understanding of the e^+e^- annihilation into hadrons. A variety of models have been used to explain the present SPEAR results, some within the context of the conventional 1^- intermediate γ state, and others with more exotic mechanisms. Questions of great importance include: (1) is there evidence for partons (jet structure, cross section decrease, etc.)? (2) does scaling hold, and over what region? (3) what is the s dependence of various exclusive cross sections? (4) what are the cross sections for production of heavier particles and how does their production vary with s?

B. QED Studies

Such a detector can clearly test QED predictions with high accuracy. More specifically it can study the reactions:

$$e^+e^- \to e^+e^-,\ e^+e^- \to \gamma\gamma,\ e^+e^- \to \mu^+\mu^-$$

For these reactions direction and momentum measurements of the charged particles in the magnetic field and energy measurements in the shower counters are sufficient for identification.

C. Search for New Particles

The search for new particles is a very exciting area since the total energy will be 30 GeV, and heavy leptons, charmed particles, Higgs scalars, quarks, gluons, etc. (if they exist) could be produced.

We will want to measure the total energy as well as the energy and momentum of individual particles. This combined with identification of electrons among the hadrons can give important clues on the production of some of the above particles. A partial list of signatures is: [1]

(a) presence of ν, i.e. missing $p_\perp$ and E,

(b) leptons mixed in with hadrons,

(c) leptons associated with strange particles,

(d) massive colinear pairs.

In the sections that follow we will discuss separately the various components of the detector and point out for each, how well they achieve the goals (a) - (e) discussed in the introduction. Detection of n and $\bar{n}$ is quite difficult and not considered worthwhile in view of the necessary compromises on the γ detection (they are expected to be 1% of all particles).

However, p and $\bar{p}$ are detected.

III. The Central Detector

The design we consider here uses a solenoidal magnet as central detector to measure direction and momenta of the charged particles and a neutral detector outside the magnet to measure direction and energy of the γ rays. The main constraints on the central detector are:

(a) Small radial dimensions of the magnet so that the volume and cost of the γ detector is kept to reasonable values.

(b) Accurate position measurement inside the magnet in order to obtain good $\vec{p}$ measurements for charged particles.

(c) Thin magnet coils to minimize the energy deposited by the showers in the coils. This is important to achieve a good energy measurement of the γ rays.

Figure 1 shows a side view of the detector. Figure 2 is a cross sectional view. The neutral detector shown corresponds to alternative A to be discussed later.

A. Charge Particle Detector

Five cylindrical double drift chambers are placed inside the solenoid to insure good momentum measurements for the charged particles. The spatial resolution of drift chambers[2] is excellent thus allowing for good momentum measurements to be made in a magnet of small radius. Recent tests[3] of small drift chambers without electric field shaping have shown that the spatial resolution is better than $\pm 75\mu$ even in a magnetic field as high as 15 KG. These results show that cylindrical drift chambers with sense wires parallel to the magnetic field and without electric field shaping can have high spatial resolution. For the large chambers considered here mechanical stability will possibly provide the limiting precision.

Figure 3 shows the uncertainty in the momentum of the charged particles calculated for B = 5 KG and B = 10 KG, including multiple scattering in the drift chambers and assuming $\Delta x = 0.1$ mm. and $\Delta x = 0.2$ mm for the position measurement. A total of 0.027 radiation length of material including styrofoam, aluminum, mylar, glue, wires, chamber and inter-chamber gas was assumed. The magnet radius was in all cases r = 0.75 meter. It appears that 5 KG is a reasonable value for the magnetic field, but that 10 KG would be desirable. The magnet parameters for conventional coils and a superconducting coil are discussed next.

B. Conventional Magnet

The design of a normal magnet involves the factors of power consumption and radiation length of coil wall. A tradeoff between these factors was made and led to a coil thickness of 5cm of aluminum. This needs 1.7 MW of power at full field (5 KG). About 35% of the γ's will convert in this coil but since the conversion is detectable by time of flight scintillator outside the coil (see Section V), the γ energy resolution will not be significantly degraded for $E\gamma > 100$ MeV. The parameters for this design are shown in Table I. The iron return yoke is designed to leave the end regions open for additional particle detectors (see Fig. 1).

C. Superconducting Magnet

An alternative magnet design considered is one which makes use of a superconducting coil in the solenoid. Niobium-titanium alloy is used for the superconductor, and this is embedded in an aluminum matrix to minimize γ conversions.* This combination forms the superconducting cable from which the coil is wound. The NbTi alloy will carry about 1.5×10^5 amps/cm^2 at 50 KG in short sample tests. There are some important factors bearing on the design which must be examined systematically with considerable care. These include: (1) the effect of hoop stress on the stability of the properties of the superconductor, and (2) the transition to the normal conducting state. The speed of propagation of the latter is important in determining the local temperature rise, which must be kept within limits. To allow a generous safety factor for uncertainties such as these, a current density of 1.0×10^4 amps/cm^2 was used, a derating factor at 10 KG of about 40 from the short sample tests.

Some estimated quantities relating to the physical parameters and cost of the superconductor are:

Properties of NbTi:

Density	$\sim$ 6 g/cm^3 (54% Nb by weight)
Radiation Length	$\sim$ 10 g/cm^2 = 1.67 cm
Absorption Length	$\sim$ 150 g/cm^2 = 25.0 cm
(Z_{Nb} = 41, Z_{Ti} = 22)	

Properties of NbTi-Al S.C. Cable:

Density	= 4.8 g/cm^3
Radiation Length	$\sim$ 2.4 cm
Absorption Length	$\sim$ 28.4 cm

+Cost of Superconducting Cable: \$50 - \$100/lb.

*At present only a copper matrix has been used in production, but there seems to be no apparent reason that aluminum would not work well also.

+As estimated by W. Gilbert, LBL Engineering Department.

The parameters of the superconducting central solenoid are given in Table I for two nominal field strengths: 5 KG and 10 KG. Most of the weight is in the iron yoke in both cases, and this is much larger at 10 KG in order to contain the increased magnetic flux. It can be seen that the coil thickness is smaller than for a conventional copper conductor at the same field strength. Some additional thickness of Al, probably about 0.1 $L_{rad} = 0.024\ L_{abs}$ must be added for the Dewar thickness. The initial cost is mostly in the cryogenic system, and not in the coil itself. The power savings over the conventional magnet are quite substantial. The hoop stresses on the conductor are about 1/6 and 1/3 of the Al yield point at 5 KG and 10 KG, respectively, without any additional support, so this does not appear to be a serious problem.

IV. Detection of Particles at Small Angles

A composite detector, consisting of the central solenoid, with aspect ratio L/R = 4 as previously considered, and a pair of toroidal coils in end regions (Fig. 1), is next considered.

A. Conventional Conductor

A one-meter long toroid, using aluminum conductor (0.6 MW/coil) or superconductor is placed 3 ± 0.5 m from interaction point at each end of solenoid, covering an angular region from about 5° to 25° (and 155° to 175°). Four high-resolution chambers (σ = 0.2 mm) inside the toroids are used, plus two between the solenoid and each toroid, the latter chambers just to insure unambiguous tracking and observation of scattering when it occurs in the entrance wall. The resulting precision in momentum measurement including multiple coulomb scattering varies from about 9% P (GeV/c) at the outer radius where B $\approx$ 1.4 KG to about 2% P (GeV/c) at inner radius where B $\approx$ 7 KG.

For the conventional aluminum conductor the wall thickness corresponds to 0.11 radiation lengths (L_{rad}) and 0.03 absorption lengths (L_{abs}) at outer radius (r_2) and 0.56 L_{rad} and 0.13 L_{abs} at inner radius (r_1). Perhaps the latter values can be reduced somewhat by an optimized design for heat transfer at inner radius, and running the wall <u>hotter</u> at this point. For superconductor, these corresponding values are 0.04 L_{rad} and 0.004 L_{abs} at r_2 and 0.23 L_{rad} and 0.02 L_{abs} at r_1 (see Table II). The relative error in momentum measurement, $|\Delta P/P|$, is unaffected by a substitution of

superconductor for aluminum, since the chambers are inside the coil. There appears to be some gain in L_{rad} and L_{int} by replacement of aluminum by superconductor. A potential advantage of the superconductor option might be that the solenoidal stray field could be totally excluded by induced currents, if the solenoidal is energized after the toroid reaches its superconducting state. If that were a practical operating mode, then only deflections in the θ direction would occur inside the toroid, simplifying the analysis. There is ample room for a 20 cm thick Cerenkov detector, for particle identification, in the (otherwise unused) fringe-field region between the solenoid and toroid. Behind the toroid may be placed lead glass blocks or other neutral particle detectors.

Time-of-flight capability may be added by placing 12-16 scintillator sectors just in front of the toroid. There is a flight path of 2.5 m from the interaction point, giving π-K separation up to 0.9 GeV/c and π-p separation up to 1.8 GeV/c, at a time separation of 4σ = 1.0 ns. Here it appears that 2" diameter phototubes are needed (and possible) only on the outer edge of these sectors. The sectors of scintillators will be matched with similar sectors in the Cerenkov counters. These are formed by the internal webs needed to support gas pressure, and form cells in which particles are separately identified. The present design has a 20 cm gas thickness (see Section V) which gives about 30 photoelectrons for a particle well above threshold, assuming a light collection efficiency of 0.25. (The gas thickness can easily be increased to $\approx$50 cm if this efficiency can not be achieved.)

B. Superconducting End Coil

The same parameters are chosen as for the previously discussed design using aluminum conductors, to have a direct comparison on relative merits. These quantities and S.C. costs are contained in Table II. The superconducting end coil appears superior in every way compared with the aluminum coil design, particularly in terms of operating (power) costs. Clearly the principal costs will not be for purchase of S.C. material, but for the cryogenics equipment.

Generally, it appears very advantageous to make both the central and end coils of superconducting materials.

V. Particle Identification

Separation of π's, K's and p's will be done by three methods; time of flight, ionization loss, and Cerenkov counting. Alternative A will use a combination of the first two methods and will be able to separate π-K up to 0.6 GeV/c and π-p up to 1.2 GeV/c. In alternative B, a high-pressure gas Cerenkov counter will be added which will extend the π-K separation up to 2 GeV/c and π-p separation up to 4 GeV/c.

Time-of-flight measurements will be made using 96 long scintillator slats (1.5 x 0.13 x 0.02 m) surrounding the magnet. The starting time will be determined by the machine beam bunch crossing time or by a pulse initiated by a particle traversing an inner cylindrical scintillator. A time resolution of $\pm$ 0.4 ns should be readily achievable with this geometry.

Ionization loss in these same scintillators will be determined from pulse height measurement. Use of this additional information should yield a mass resolution somewhat better than that given by time-of-flight alone. Pulse height resolution of $\pm$0.1 is assumed possible.

For alternative B, a 20 cm thick gas Cerenkov counter will surround the magnet (Figure 4, 5). This counter will run with Freon 13 at approximately 25 bars pressure, corresponding to an index of refraction of 1.03. Radial vanes will separate the counter into 36 azimuthal regions. These vanes (2 mm thick) will provide the necessary strength to allow the innerwall thickness to be small. The total thickness of the counter will be about 0.2 X_0 of Al. For β = 1 and a geometrical light collection efficiency of .25 one should detect about 30 photoelectrons. The light collection scheme would have curved, reflective surfaces inside each section to minimize losses. With this design, the stated separation should be easily achieved.

One appealing aspect of the gas Cerenkov counter proposed here is its ability to cover a wide range of refractive indices and still achieve high efficiency. By raising the pressure of Freon 13 to 33 bars, one can achieve an index of refraction of 1.05, although at this pressure, temperature control of the gas would be necessary. At this high pressure, π-K separation extends as low as 0.45 GeV/c, thus providing substantial overlap with the upper end of the TOF and dE/dx systems where these begin to lose discrimination power. At a pressure of 12 bars (n = 1.01), and for β = 1, the counter will still yield 10

photoelectrons and thus resolve π - (K, p) up to 4 GeV/c and (π,K) - p up to 7 GeV/c, although a gap in π-K separation exists from about 0.6 to 1.0 GeV/c caused by the limits of the time of flight and ionization loss techniques.

Details of design considerations and kinematics are given in the note by Mast and Nelson.[4]

VI. Gamma Detector

The best energy resolution in γ detection is obtained with NaI, Pb glass and liquid argon detectors.[5] Of these the first two have been used in many experiments and have well known properties. Liquid argon detectors are still being developed. The energy resolution is (E in GeV):

$$\frac{\Delta E}{E} = \frac{1\%}{E^{\frac{1}{4}}} \qquad \text{for NaI}$$

$$\frac{\Delta E}{E} = \frac{5\%}{\sqrt{E}} \qquad \text{for Pb glass}$$

$$\frac{\Delta E}{E} \lesssim 5\% \qquad \text{for liquid argon}$$

For liquid argon the resolution is limited by amplifier noise at low energy and by shower energy-loss fluctuations at high energy. NaI is certainly the best but it is also the most expensive, a factor of five more expensive then Pb glass for the same volume. The cost of a liquid argon detector is less easy to evaluate.

A. Resolution of π° mass

In trying to reconstruct π°'s from the measurements of the shower energies and positions the following formulae are relevant :

$$M^2 = 2E_1E_2(1-\cos\theta_{\gamma\gamma})$$

$$\frac{dM}{M} = \frac{1}{2}\left[\left(\frac{4E_1E_2}{M^2} - 1\right) d^2\theta_{\gamma\gamma} + \left(\frac{dE_1}{E_1}\right)^2 + \left(\frac{dE_2}{E_2}\right)^2\right]^{1/2}$$

where E_1 and E_2 are the energies of the two γ rays and $\theta_{\gamma\gamma}$ their opening angle. Notice that both energy and position resolution are important. For the liquid argon detector the position resolution will be discussed in Section VI C. For NaI and Pb glass it depends on the particular experiment

arrangement. Figure 6 shows the curves of $\frac{dM}{M}$ as function of momentum for dx = 0.5 cm at a distance r = 0.85 m (see reference 4 for a description of how the curves were obtained). The largest difference between the two types of detectors is seen below 2 GeV/c.

B. Lead Glass Gamma Detector

Gammas are detected by a cylindrical array of lead glass blocks and multi-wire proportional chambers. The configuration shown in Figures 1 and 3 consists of two layers of active converter followed by $9X_0$ of lead glass blocks. Each layer of active converter consists of a layer of lead glass counters (1.6 radiation lengths thick) followed by a multi-wire proportional chamber. The energy deposited in each layer is measured, and the point of conversion is determined in the wire chambers. Following the active convertors is a matrix of lead glass blocks which measure the energy remaining in the shower. This configuration has good energy resolution (δ E/E = 0.05/$\sqrt{E(GeV)}$)[6] and gives the good spatial resolution ($\pm$ 0.5 cm) required for the reconstruction of π^0's. The lead glass array is divided azimuthally about the beam into 48 wedges and symmetrically about the interaction point. The active converters and end blocks are viewed from each end of the system. The central blocks are view radially. There are 96 counters in each layer of active converter and 768 outer blocks requiring a total of 960 phototubes. The total volume of the lead glass is 8.0 m^3 costing about \$800K. The cost of phototubes and associated electronics would be about \$300K.

Adding gamma detection to the small angle detectors significantly increases the lead glass requirements. The solid angle is small but the glass is necessarily at a large distance from the interaction point. The array shown in Figure 1 for <u>one</u> end of the detector requires 3.7 m^3 of glass costing about \$370K. The cost of phototubes and associated electronics would be about \$140K.

C. Liquid Argon Gamma Detectors with Gas Cerenkov Counters

With the introduction of the gas Cerenkov counters the cost of using lead glass for gamma detection becomes prohibitive. It seems reasonable to expect that by the time PEP is running new and less expensive detectors will have been developed. At the moment the liquid argon ionization counter looks very promising. The successful testing of liquid argon counters by Engler, et al. and Willis and Radeka[7] is encouraging. A possible design

for an argon counter to look at gamma showers is briefly discussed by Al Odian in a paper for this Summer Study.[5]

Since the present experience with such detectors is so limited we can only roughly sketch what such a detector might look like. We follow Odian's design using mylar sheets with square detectors perpendicular to the gamma direction in a tank of pure liquid argon (i.e.,without converter plates). Tanks 10 radiation lengths thick (X_0 = 14 cm) will be arranged azimuthally around the magnet. Including end cap chambers the total volume of argon for an almost 4π detector is about 85 m^3 costing about \$15K.

In order to get good spatial resolution ($\sim \pm$ 1 cm) and have a small electron collection time the detecting squares are spaced every 2 cm throughout the liquid. About 50,000 columns of connected squares will be required. The major cost of the detector will be in the cryostats and readout. A very rough estimate of the cryostats gives about \$100 K. but this of course depends on the quality of insulation and refrigeration available. Using present technology to build a sample and hold for each column, multiplexers for each 100 columns, and an amplifier and ADC (or two) for each multiplexer, we estimate the readout would cost today between \$175K and \$250K. The readout represents the bulk of the detector cost,and we are hopeful that 5 years of rapid developments in electronics will reduce this cost. The energy resolution is better than lead glass but would be limited here by shower leakage fluctuations to about $5\%/\sqrt{E}$ above 1 GeV.

VII. Triggering and Background Rates

The important criteria in designing a triggering scheme are: (1) selecting the events of interest in a bias-free way, and (2) suppression of background events. The expected muon pair production rate is 0.01/sec at design luminosity ($10^{32}/cm^2$ - sec), and the Bhabha rate is 0.2/sec. The hadronic rate is not known,but at $\sqrt{s}$ = 5 GeV the ratio to muon pairs is about six. Rates have been estimated by B. Richter.[8]

Two important background sources can be predicted. These are: (1) cosmic rays and (2) the 2γ annihilation process, $e^+e^- \rightarrow e^+e^- + X$, where X is the C = +1 state formed by the two-photon interaction, and dominantly $X \rightarrow e^+e^-$.

The cosmic ray rate will be limited by requiring a coincidence between the inner drift chamber 1 m long, and the trigger scintillation counters or outer drift chamber. The rate is then approximately determined by the projected area

of the inner chamber (1.0 x 0.25 m), the gate length of the counter or chamber ($\sim$20 ns) and the e^+e^- beam collision rate (0.42 MHz). The result is about 0.34/sec. Thus beam collision events will constitute a large fraction of the triggers (at SPEAR, they are only $\sim$ 5% - 10% of all triggers).

The 2γ rate is more difficult to calculate. Hadrons produced peak strongly along the beam direction and hence this process may be suppressed or enhanced by eliminating, or using, the trigger counters in the end regions. If study of the 2γ process is a goal of the experiment, then coverage in the ends should be part of the overall trigger logic; however, if only the direct annihilations are to be studied, the trigger in the angular region 26° - 154° would probably be used. By triggering only in the latter region, an estimated 2γ rate is about one event per sec, allowing for a 60 MeV/c cutoff in P , due to curvature in the 5-KG field. The accidental rate of scattered beam electrons resulting from the 2γ events is small, estimated to be about 10^{-4} per trigger.

A basic triggering scheme which appears to be feasible is then a requirement of two or more charged particles through the inner drift chamber and scintillation trigger counters (solenoid and toroid counters). A parallel trigger might perhaps be some number of large pulses or some minimum total energy in the γ detectors. This would record, among other topologies, the annihilation into all neutral particles, a process not otherwise detected. Since the central detector covers 90% of the total solid angle, this is adequate coverage to avoid serious trigger biases and resulting model-dependent uncertainties in the interpretation of results.

VIII. Summary and Conclusions

A quantitative summary of the most important parameters and properties of the detector facility is given in Table III. In particular, the minimum requirements for the experimental area are shown.

The detector design incorporates certain features which are largely lacking in present e^+e^- colliding beam detectors. Perhaps the most important of these are: (1) the detection and measurement of γ-rays, and (2) event triggering over nearly 4π solid angle.

To construct a γ detector of reasonable cost with maximum resolution while adequately measuring charged particle momenta required a number of compromises. The solenoid magnet was made small to minimize the γ detector volume while giving some momentum resolution and reliable charge determination at the highest expected particle energies. The small size chosen (R=0.75 m) requires precise charged particle position measurements. This is achieved by

placing five drift chambers with spatial resolutions of 0.1 - 0.2 mm inside the solenoid. In the region below 2 GeV/c the momentum resolution is quite good ($\sim$5%; see Fig. 2).

The γ detectors use either lead glass or liquid argon. Achieving the intrinsic energy resolution of either of these devices (for lead glass $\frac{\Delta E}{E} = 5\%/\sqrt{E}$) requires that the γ's lose little of their energy traversing the solenoid coil. This forces the coil to be as thin as possible consistent with magnetic field and power requirements. The 5 cm Al coil thickness satisfies these constraints. Because the power demands are still rather high, a superconducting coil has also been investigated and appears feasible, although development is necessary.

A solid angle approaching 99% is achieved by keeping the end regions of the solenoid free from iron and installing a toroidal magnet system in this area. Again, because of the relatively high power demands, a superconducting toroidal magnet has also been investigated. The large solid angle provides a maximum of information for event analysis and also insures an event trigger almost free from biases by allowing essentially all e^+e^- interactions to be identified and recorded.

Particle identification makes use of time-of-flight and pulse height in a set of scintillators (Fig. 5). Kaons can be identified in this way up to a momentum of about 600 MeV/c, and protons up to about 1.2 GeV/c. By adding to the detector a 0.2 m thick gas Cerenkov counter using Freon-13, it seems possible to extend kaon identification up to about 2 GeV/c, and to tag protons in the range 2 to 4 GeV/c.

The system described here is well suited to study a very wide range of e^+e^- physics, including QED tests, inclusive, exclusive and total hadronic cross sections. For example, correlations between charged and neutral particles can be analyzed in detail to identify resonances and study their role in the annihilation process. The charged and neutral particle identification together with large solid angle coverage is well adapted to the search for new particles. The detector described here is a very powerful facility capable of studying most aspects of the anticipated as well as conjectured behavior in e^+e^- collisions at PEP.

References

1. See the report on "New Particle Searches" at this Summer Study, PEP-173.
2. G. Charpak et. al. Nucl. Inst. and Methods, 80, 13 (1970);G. Charpak et. al, Nucl. Inst. and Methods, 108 , 13 (1972); A.H. Walenta et al, Nucl. Inst. and Methods 92, 373 (1971).

3. B. Sadoulet and A. Litke, Lawrence Berkeley Laboratory Report LBL-3316 (Submitted to Nuclear Instruments and Methods)

4. T. Mast and J. Nelson in "Some Design Considerations for a Large Solid Angle Charged Plus Neutrals Detector for e^+e^- Storage Rings", a report at this Summer Study, PEP-153.

5. Report to this Summer Study "Properties of Some Photon Detectors" edited by D. Yount, PEP-155. Report to this Summer Study "Liquid Argon Gamma Ray Detectors" by A. Odian, PEP-156.

6. C.A. Heusch, R.V. Kline, C.Y. Prescott, and S.J. Yellin. Dubna Conf. on Instrumentation for High Energy Physics, USSR (Sept. 1970).

7. W.J. Willis and V. Radeka. Brookhaven National Laboratory Report BNL 18813. J. Engler, et. al. "A Liquid Argon Calorimeter for Detection of Electromagnetic and Hadronic Showers." April, 1974, submitted to Nuclear Instruments and Methods.

8. B. Richter,"Event rates to be expected at PEP", at this Summer Study, PEP-140.

Table I Central Solenoid

	Superconducting		Conventional
B(KG)	5	10	5
R(m)	.75	.75	.75
l(m)	3	3	3
θ(degrees)	26-154°	26-154°	26-154°
$\Delta\Omega$	90%	90%	90%
h(cm) (coil thickness)	0.445	0.89	5
$h^*(L_{radiation})$	0.3	0.5	.5
$h^*(L_{absorption})$	0.05	0.06	.13
Pressure from field (atm)	1	4	1
Power $^+$(MW)	.2	.2	1.8
Weight (M Tons)	50	100	50
Cost of Cryosystem	$155K	$330K	
Cost of S.C. Cable	$70 K	$130 K	
Total Cost	$225K	$460K	$50K
Electricity Cost	-	-	≈ $60K/year†

*includes dewar

+including compensating coils

†assumes 1¢/KWH, 40% duty cycle

Table II. Summary of Toroidal Analyzer

Inside (clear space) dimensions:

		Subtended angle at interaction point
Length	1 meter	
Inner radius, r_1	0.25 meter	$\Theta_{min} = 5°$
Outer radius, r_2	1.50 meter	$\Theta_{max} = 25°$

Approximate measuring precision (assuming chamber precision of 200 microns):

Trajectory Polar Angle	Entrance Radius (cm)	Field Strength (KG)	$\frac{\Delta P}{P}$ = const. P (GeV/c)
$\Theta_{min} = 5°$	25	7.0	0.02
$\bar{\Theta} = 15°$	75	4.2	0.05
$\Theta_{max} = 25°$	125	1.4	0.09

Properties of End Toroids (each end): $I = 0.85 \times 10^6$ amps

	Aluminum Conductor				Superconductor (NbTi)		
Component	h(cm)	$h(L_{rad})$	$h(L_{abs})$	$\frac{power}{coil}$(KW)	h*(cm)	$h^*(L_{rad})$	$h^*(L_{abs})$
Entrance wall							
$\Theta_{min} = 5°$	5	0.56	0.13		0.54	0.23	0.019
$\bar{\Theta} = 15°$	3	0.33	0.08	256	0.33	0.14	0.012
$\Theta_{max} = 25°$	1	0.11	0.03		0.11	0.04	0.004
+Exit wall	12.5-2.5	1.4-0.28	0.34-0.07	102	0.54-0.11	0.23-0.04	0.02-0.004
Inner conductor	10	1.1	0.27	160	0.54	0.23	0.019
Outer conductor	5	0.56	0.13	50	0.11	0.04	0.004
	Total power = 568				Material (S.C.) cost = $5,100/coil		

Estimated Total Cost $460K

Pressures are: 2 atmospheres at r_1
0.1 atmosphere at r_2

*Not included is thickness of helium Dewar walls, and this must support field pressure as indicated in Tables. An estimated thickness is 0.1 L_{rad} = 0.026 L_{abs}. The current density assumed is 10^4 amps/cm^2, as for the solenoid.

+Exit wall is 2.5 times thicker in present design, but may be made thinner at cost of power.

Table III Parameters of Detector and Requirements of Experimental Area

	Central Detector Only (a)	Central Detector Only (b)	Toroidal Analyzers
Total Cost (M$)	2	2.5	1.7
Total Weight (tons)	100	250	40
Size: Length (m.)	±4.5	±4.5	±6
Height (m.)	±2.5	±3.0	±2.5
Width (m.)	±2.5	±3.0	±2.5
Power (MW)	1.7	.2	1.2 - .1 (c)
Crane Capacity	20	20	20
No. Cables, Counters	3000	3000	2000
Drift Chambers	100	100	100
Diameter of Coil		1.5 m.	0.5 m. (r_1) 3.0 m. (r_2)
rms of momentum measurements			
$\frac{\Delta p}{p}$ for charged particles ($P \leq 2$ GeV/c)	≤8%	≤4%	2 - 10%
$\frac{\Delta E}{E}$ for γ rays (E in GeV)	$\frac{.05}{\sqrt{E}}$	<5%	$\frac{.05}{\sqrt{E}}$
Particle Identification			
π - K (P in GeV/c)	$\leq$ .6	$\leq$ 2	$\leq$ 2
π - p (P in GeV/c)	$\leq$ 1.2	$\leq$ 4	$\leq$ 4
Dangerous Gases	Isobutane for drift chambers		

(a) Conventional magnet, lead glass γ detector

(b) Superconducting magnet, liquid argon γ detector.

(c) Two values correspond to conventional or superconducting magnet

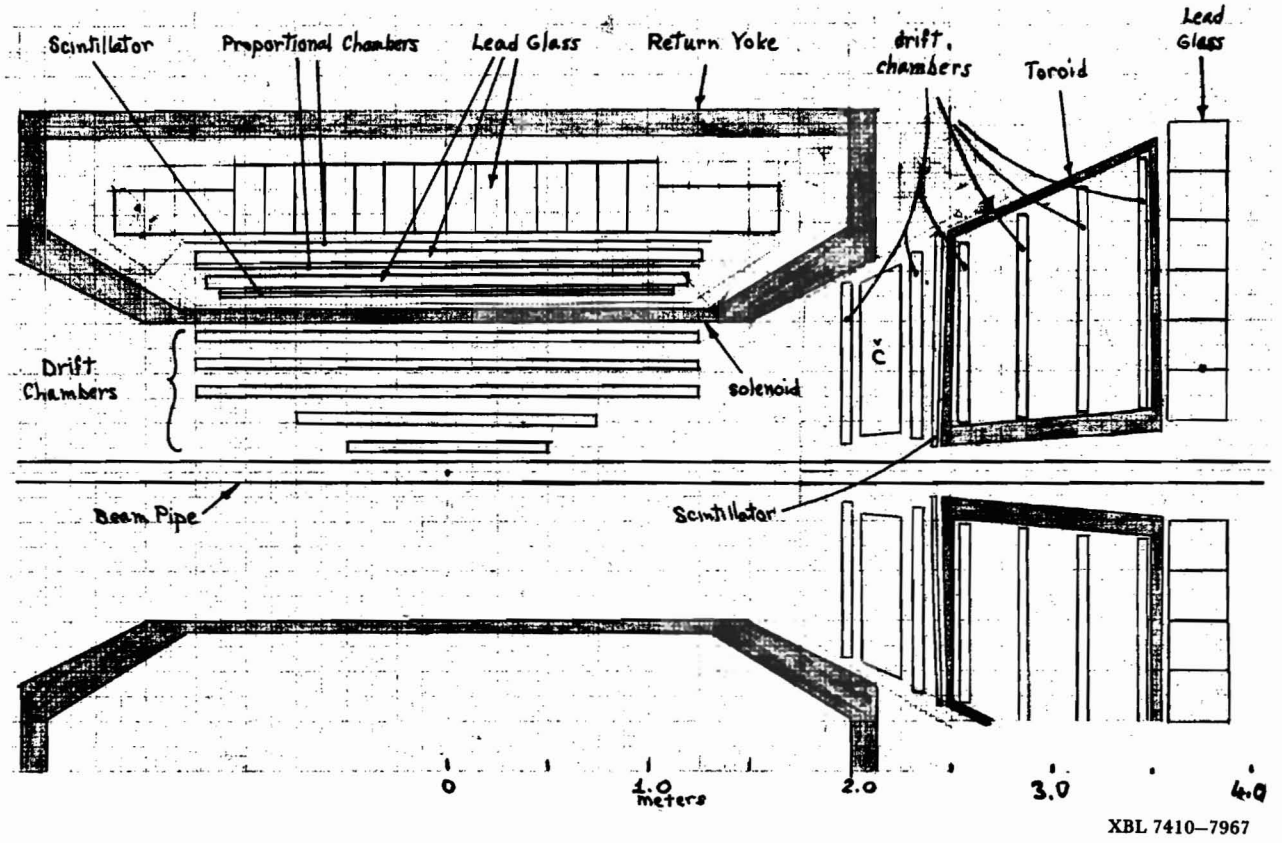

Figure 1. A side view of the detector. Blackened areas represent magnet coils. C is a Cerenkov counter, the other detectors are indicated. This sketch refers to Alternative A, which uses Pb-glass shower counters. The scale is shown at the bottom of the figure.

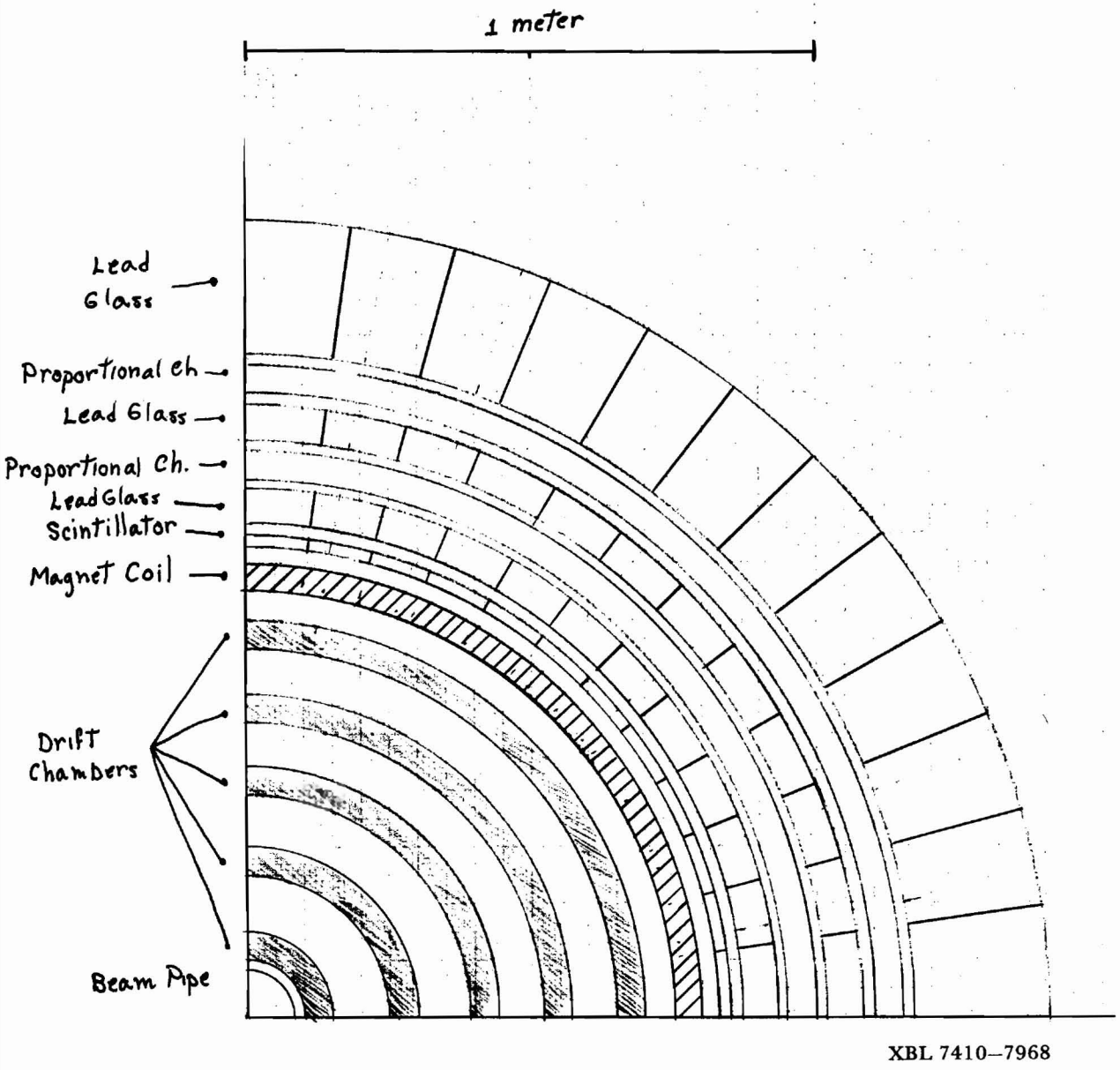

Figure 2. Cross section of the detector shown in Figure 1. Only one quadrant of alternative A (Pb-glass γ detector) is shown.

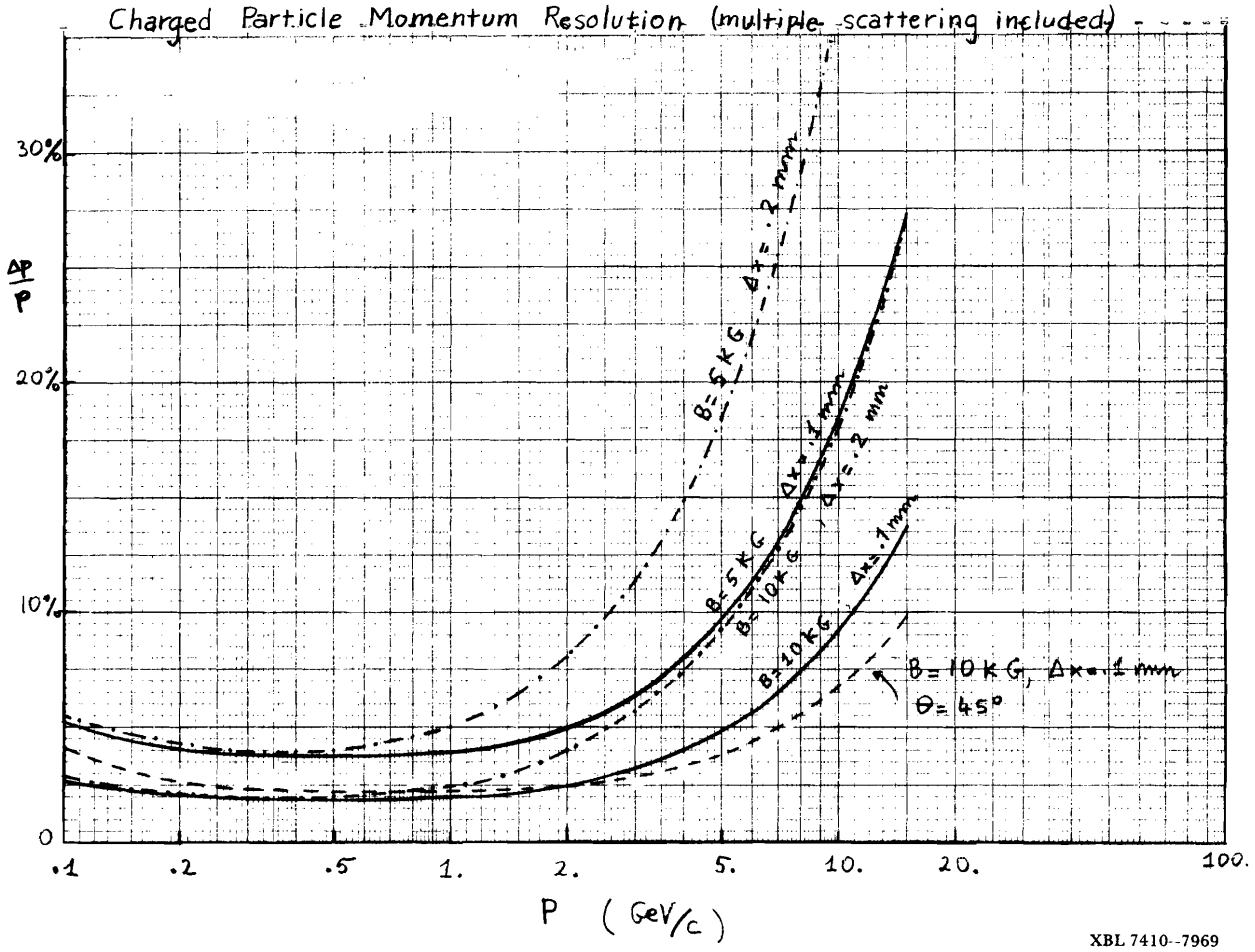

Figure 3. Momentum resolution of charged particles for different values of magnetic field, B. Also different position resolution in the drift chambers $\Delta x = 100\mu$ and $\Delta x = 200\mu$ are considered. All curves, except one, refer to normal incidence, $\theta = 90°$.

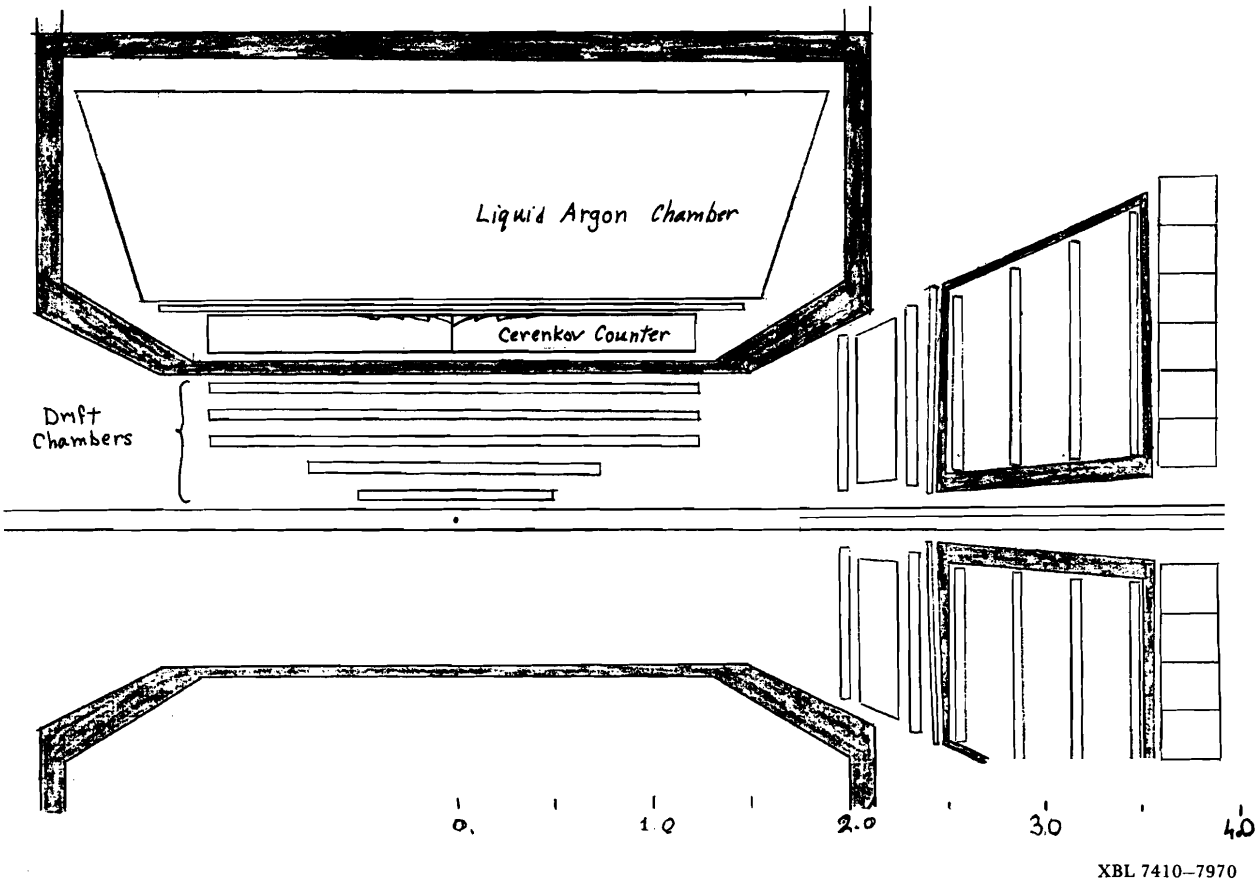

XBL 7410–7970

Figure 4. Side view of the detector for alternative B. The Cerenkov counters and Liquid Argon chamber are shown, the rest is as in Figure 1.

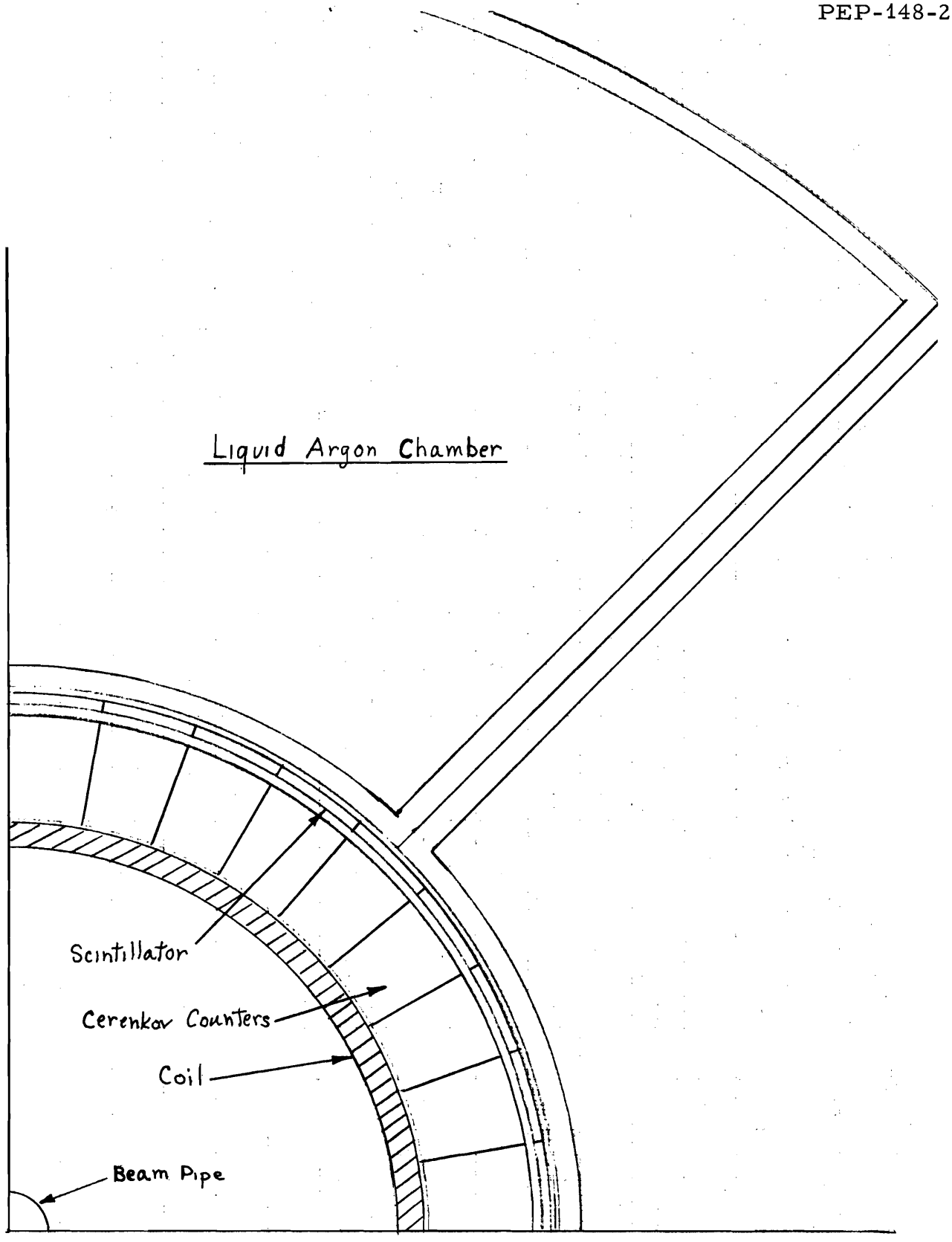

XBL 7410–7971

Figure 5. Cross section of the detector shown in Figure 4. Only one quadrant of alternative B (liquid Argon γ detector) is shown.

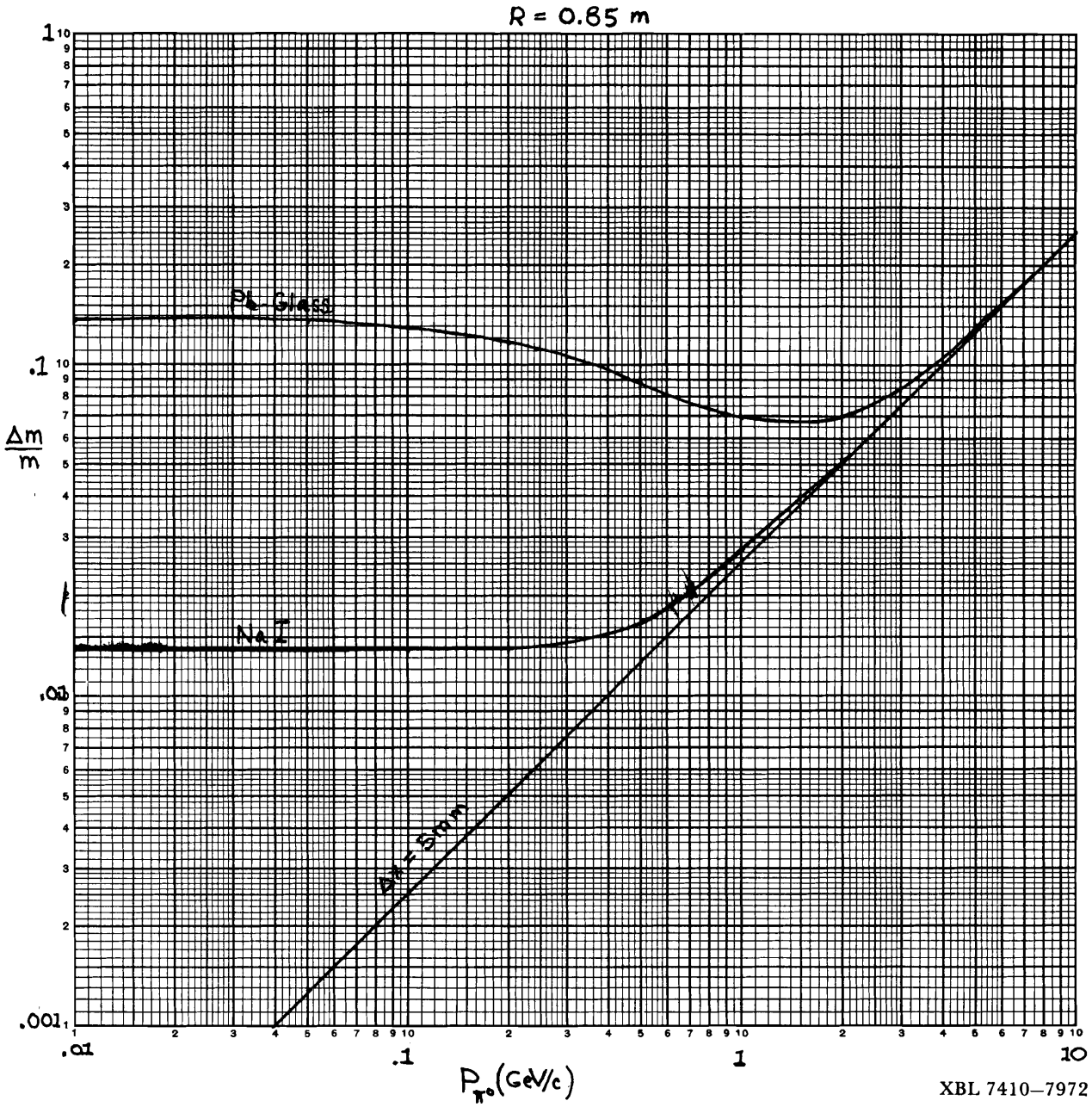

Figure 6. π° mass resolution for a γ spatial resolution of 5 mm at R = 0.85 m and various assumed γ energy resolutions.